Atmospheric Environment 69 (2013) 345–353

Contents lists available at SciVerse ScienceDirect

Atmospheric Environment

journal homepage: www.elsevier.com/locate/atmosenv

Remote sensing of exposure to NO_2: Satellite versus ground-based measurement in a large urban area

Matthew J. Bechle [a], Dylan B. Millet [a,b], Julian D. Marshall [a,*]

[a] Department of Civil Engineering, University of Minnesota, Minneapolis, MN 55455, USA
[b] Department of Soil, Water, and Climate, University of Minnesota, Minneapolis, MN 55455, USA

HIGHLIGHTS

- We estimate satellite-based surface NO_2 concentrations from the OMI sensor.
- We compare OMI estimates with ground-based in situ measurements in a large urban area.
- Within-urban spatial signature of surface NO_2 is well resolved by OMI column measurements.
- OMI provides a useful dataset for exploring the epidemiological impact of urban air pollution.
- OMI measurements may be a useful tool for exploring NO_2 variability between urban locations.

ARTICLE INFO

Article history:
Received 29 October 2011
Received in revised form
16 November 2012
Accepted 20 November 2012

Keywords:
OMI
Nitrogen dioxide
Urban air quality
Remote sensing
Exposure

ABSTRACT

Remote sensing may be a useful tool for exploring spatial variability of air pollution exposure within an urban area. To evaluate the extent to which satellite data from the Ozone Monitoring Instrument (OMI) can resolve urban-scale gradients in ground-level nitrogen dioxide (NO_2) within a large urban area, we compared estimates of surface NO_2 concentrations derived from OMI measurements and US EPA ambient monitoring stations. OMI, aboard NASA's Aura satellite, provides daily afternoon (~13:30 local time) measurements of NO_2 tropospheric column abundance. We used scaling factors (surface-to-column ratios) to relate satellite column measurements to ground-level concentrations. We compared 4138 sets of paired data for 25 monitoring stations in the South Coast Air Basin of California for all of 2005. OMI measurements include more data gaps than the ground monitors (60% versus 5% of available data, respectively), owing to cloud contamination and imposed limits on pixel size. The spatial correlation between OMI columns and corrected in situ measurements is strong ($r = 0.93$ for annual average data), indicating that the within-urban spatial signature of surface NO_2 is well resolved by the satellite sensor. Satellite-based surface estimates employing scaling factors from an urban model provide a reliable measure (annual mean bias: −13%; seasonal mean bias: <1% [spring] to −22% [fall]) of fine-scale surface NO_2. We also find that OMI provides good spatial density in the study region (average area [km^2] per measurement: 730 for the satellite sensor vs. 1100 for the monitors). Our findings indicate that satellite observations of NO_2 from the OMI sensor provide a reliable measure of spatial variability in ground-level NO_2 exposure for a large urban area.

Published by Elsevier Ltd.

1. Introduction

Urban air pollution is one of the top 15 causes of death and disease globally (top 10 for high-income countries), responsible for an estimated 1 million deaths annually (Mathers et al., 2009). Nitrogen dioxide (NO_2) is an important component of urban air pollution and a precursor to ground-level ozone, particulate matter, and acid rain. Epidemiological studies have linked NO_2 to several adverse health effects (Brauer et al., 2008; Kim et al., 2004), including cardiopulmonary mortality (Beelen et al., 2008), lung cancer (Filleul et al., 2005), and asthma exacerbations (Castellsague et al., 1995; Gauderman et al., 2005). The lifetime of NO_2 against oxidation in the troposphere is short (~hours), leading to large spatial variability near sources (Hoek et al., 2008; Liang et al., 1998; Madsen et al., 2011; Marshall et al., 2008; Novotny et al., 2011). Quantifying the spatial variability in surface NO_2 concentrations provides valuable information for air pollution exposure assessment and environmental justice. Here we examine how well satellite-based measurements of NO_2 from the Ozone Monitoring Instrument (OMI) can resolve spatial variability in ground-level concentrations within a large urban area, and to what degree

* Corresponding author. Tel.: +1 (612) 625 3297; fax: +1 (612) 626 7750.
E-mail address: julian@umn.edu (J.D. Marshall).

1352-2310/$ – see front matter Published by Elsevier Ltd.
http://dx.doi.org/10.1016/j.atmosenv.2012.11.046

scaling factors (surface-to-column ratios) from local or global chemical transport models provide an additional constraint.

The spatial resolution of ground-based measurements is constrained by the limited number of monitors and their proximity. High quality in situ measurements are frequently lacking in developing countries. Remote sensing of air pollution can supplement existing ground-based monitors and provide coverage where ground-based data are unavailable (Brauer et al., 2012; van Donkelaar et al., 2010). Satellite observations of tropospheric NO_2 column abundance have been conducted since 1995 (Burrows et al., 1999) and have been improving in spatial and temporal resolution (Martin, 2008). Methods to relate these remotely sensed column abundances to surface concentrations are necessary for satellite measurements to inform discussions on air pollution and attributable health effects. Ground-level NO_2 concentrations obtained from OMI on the basis of surface-to-column ratios simulated with a chemical transport model (CTM) have been shown to agree well with corrected in situ measurements in the US and Canada (Lamsal et al., 2008, 2010). That finding suggests that OMI can detect regional variability in NO_2. Much of the research comparing satellite and ground-level measurements of NO_2 has focused on temporal (Ghude et al., 2011; Kramer et al., 2008; Meng et al., 2010; Petritoli et al., 2004; Russell et al., 2010) or spatio-temporal (Boersma et al., 2009; Lamsal et al., 2008, 2010; Ordoñez et al., 2006) patterns, and focused on large spatial scales (Blond et al., 2007; Duncan et al., 2010) and/or rural locations. Studies that have focused on urban NO_2 are limited to a single monitor (Boersma et al., 2009; Ghude et al., 2011; Petritoli et al., 2004) or a spatial average (Kramer et al., 2008; Russell et al., 2010) for the urban areas examined. Limited work has been done to evaluate the ability of OMI or other current satellite sensors to detect gradients of surface NO_2 within a single urban area. In addition, modeled NO_2 is susceptible to biases in coarse-resolution chemical transport models, owing to non-linearity in NO_2 chemistry. Valin et al. (2011a) found that a model resolution of 4–12 km is necessary to predict NO_2 column abundance with 10% accuracy. To our knowledge no research has evaluated the role of model resolution in estimating surface-to-column ratios for interpreting satellite measurements. See Table S1 in the Online Supplemental Information (SI) for a summary of articles comparing satellite and ground-level measurements of NO_2.

Here, we compare satellite and ground-based measurements of NO_2 in California's South Coast Air Basin (SoCAB) to evaluate the spatial fidelity of OMI measurements in a large urban area. We evaluate three potential scaling factors (i.e., surface-to-column ratio) – a "constant" factor, based on typical urban conditions; and, spatio-temporally varying factors based on global- (GEOS-Chem) and urban-scale (CAMx) chemical transport models. We compare the resulting satellite-derived estimates to in situ measurements of surface concentrations in order to evaluate the ability of OMI to capture gradients of ground-level NO_2 within a large urban area, and to assess the role of model resolution in deriving estimates of surface NO_2 from satellite data. The South Coast provides a logical study location because of the large number of NO_2 monitors, because chemical transport models such as CAMx are well developed for this urban area, because of the generally sunny climate (minimizing data contamination by clouds), and because of the large population exposed to poor air quality.

2. Methods

2.1. OMI data

The OMI sensor (Levelt et al., 2006) aboard the Earth Observing System (EOS) Aura satellite provides daily global measurements of tropospheric NO_2 column abundance. The satellite follows a sun-synchronous orbit, passing over each location at ~13:30 local time (Schoeberl et al., 2006). OMI takes 60 cross-track measurements along a 2600 km swath with nadir resolution up to 13×24 km^2. The OMI nadir pixel observes the same location every 16 days; the center point and pixel size at a given location differs by day during this cycle. Adjacent OMI pixels along the flight path also exhibit slight overlap at the edges of the swath, so the effective spatial resolution of OMI observations increases with temporal averaging. We use the OMI Standard Product (Version 1.0.5, Collection 3) from the NASA Goddard Earth Sciences Data and Information Services Center (GES DISC) (available: http://disc.gsfc.nasa.gov/Aura/OMI/omno2_v003.shtml). We use data from 2005, when emission inventories for CAMx are available (Ospital et al., 2008). Details regarding the OMI NO_2 Standard Product are available elsewhere (Boersma et al., 2002; Bucsela et al., 2006; Celarier et al., 2008). Briefly, retrievals rely on the determination of slant column densities calculated by differential optical absorption spectroscopy in a spectral window specific to NO_2 (405–465 nm). A background (stratospheric) NO_2 field is determined by applying masks over areas with high tropospheric NO_2 column abundance, smoothing the remaining data, and performing a zonal planetary wave analysis up to wave-2. Slant columns are then converted to tropospheric vertical column densities using a tropospheric air mass factor (AMF) that accounts for vertical profiles of temperature and NO_2 (the latter based on an annual average profile as simulated by GEOS-Chem), viewing geometry, and the pressure and reflectivity from clouds and terrain. Cloud top height and cloud fraction are obtained from OMI using the O_2–O_2 algorithm (Acarreta et al., 2004).

The main sources of error in determining tropospheric NO_2 columns are associated with uncertainties in surface albedo, aerosols, cloud parameters, and the NO_2 vertical profile (Martin et al., 2002; Boersma et al., 2004). Recent work employing high spatial and temporal resolution terrain, albedo, and profile inputs suggest that the coarse resolution of these inputs in the standard OMI product lead to an overestimation of tropospheric NO_2 (~30%) for relatively clean regions and an underestimation (~8%) for urban regions (Russell et al., 2011). Additional errors arise in resolving stratospheric from tropospheric NO_2, resulting in an estimated overall error in tropospheric NO_2 column density of up to 30% for clear scenes and up to 60% for scenes in the presence of clouds or haze (Boersma et al., 2002). Lamsal et al. (2008, 2010) also found that the OMI Standard Product exhibits a seasonal bias, owing to the use of an annual average NO_2 profile to calculate the AMF. The reported amplitude of the seasonal bias is larger for rural locations (74% [summer] versus −6% [winter]) (Lamsal et al., 2010) than for urban locations (−17% [summer/fall] versus −36% [winter/spring]) (Lamsal et al., 2008). To minimize errors associated with cloud cover, we use here only cloud-free scenes (cloud radiance fraction <0.3). To reduce spatial averaging near the swath edge, we only use pixels with footprint area <1200 km^2. We eliminate measurements with a root mean square error of fit greater than 0.0003, with solar zenith angle greater than 85°, and according to data-quality flags provided with the data product.

2.2. Surface-to-column scaling factors

Determining ground-level concentrations of NO_2 from OMI tropospheric column abundance requires knowledge of the local vertical profile of NO_2. Lamsal et al. (2008, 2010) showed that the NO_2 vertical profiles obtained from a global three-dimensional chemical transport model (GEOS-Chem) can be used to estimate ground-level NO_2 concentrations from OMI tropospheric NO_2 column observations, with significant temporal correlation ($r = 0.3$–0.8 across the US and Canada) versus observations. Here, we focus on

evaluating the extent to which OMI can resolve fine-scale NO_2 gradients within a large urban area. We start with a single assumed typical urban profile as a straightforward baseline method to convert column measurements to surface estimates. We also employ more detailed approaches, with urban (CAMx) and global (GEOS-Chem) models providing spatially and temporally -specific estimates of the NO_2 vertical profile. Spatial precision is 2×2 km^2 for CAMx and $2 \times 2.5^\circ$ (roughly 220×230 km^2 in the SoCAB) for GEOS-Chem. While the global-scale model provides no significant spatial information on the scale of the SoCAB, we include it here to assess whether the temporal information provided (day-to-day variability in scaling factors) offers an improvement relative to the single-profile approach.

2.2.1. GEOS-Chem model

We use the GEOS-Chem global three-dimensional model of atmospheric chemistry (version 8, http://www.geos-chem.org) to provide a global-scale simulation of NO_2 and its vertical distribution. GEOS-Chem uses GEOS-5.2.0 assimilated meteorological data from the NASA Goddard Earth Observing System, which have 6-h temporal resolution (3-h for surface variables and mixing depths), $0.5 \times 0.667^\circ$ horizontal resolution, and 72 vertical layers. For computational expediency we degrade the horizontal resolution here to $2 \times 2.5^\circ$ and the vertical resolution to 47 vertical layers. The model includes detailed ozone–NO_x–VOC chemistry coupled to aerosols, with 120 species simulated explicitly. Boundary layer mixing in GEOS-Chem uses the non-local scheme of Lin and McElroy (2010). Further details regarding the model simulation for NO_2 and related species, including evaluation against aircraft and surface data, are provided elsewhere (Hudman et al., 2007). Anthropogenic emissions over the US are from the Environmental Protection Agency (EPA) 1999 National Emission Inventory (US EPA, 2008), with adjustments described by Hudman et al. (2007, 2008) to account for recent reductions. We use GEOS-Chem output averaged during a 3-h window (12:00–15:00 local time) corresponding with the Aura overpass for each day.

2.2.2. CAMx model

We use the Comprehensive Air-Quality Model with extensions (CAMx, http://www.camx.com/) to provide an urban-scale (2×2 km^2 grid cells) simulation of year-2005 NO_2. We employ hourly meteorological data from MM5 (http://www.mmm.ucar.edu/mm5/) mesoscale meteorological model, generated using four dimensional data assimilation and National Weather Service model initializations. We employ the MATES III emissions inventory, developed by the South Coast Air Quality Management District (SCAQMD). A detailed description of the meteorological inputs and emissions inventory can be found elsewhere (Ospital et al., 2008). CAMx includes 8 vertical layers from the surface (1000 hPa) to ~2 km (800 hPa). Vertical mixing in CAMx is driven by the Eulerian continuity equation closed by K-theory. We employ Carbon Bond Mechanism IV for gas-phase chemistry mechanisms. Boundary and initial conditions were obtained from the 2005 annual simulations used for the SCAQMD's 2007 Air Quality Management Plan compliance demonstration (SCAQMD, 2007). Of particular relevance for our application is the vertical boundary atop the CAMx domain, which for NO_2 is constant at 0.02 ppb. As with GEOS-Chem, we averaged CAMx hourly NO_2 concentrations to correspond with Aura/OMI overpass (12:00–15:00 local time).

2.3. Ambient monitoring station data

We employ publicly available hourly in situ NO_2 measurements from the US EPA. We calculate the average over the satellite overpass time (12:00–15:00 local) for each of the 25 ground-level NO_2 monitors located in the study region (Fig. 1). All monitors employ chemiluminescence analyzers, which measure NO_2 indirectly as the difference between alternating measurements of nitric oxide (NO) and nitrogen oxides ($NO_x \equiv NO + NO_2$) (US EPA, 1975). The reaction of NO with ozone produces a characteristic chemiluminescence that allows for the direct measurement of NO in the sample. NO_x is then measured in the same way after passing the incoming air over a molybdenum converter that reduces NO_2 to NO.

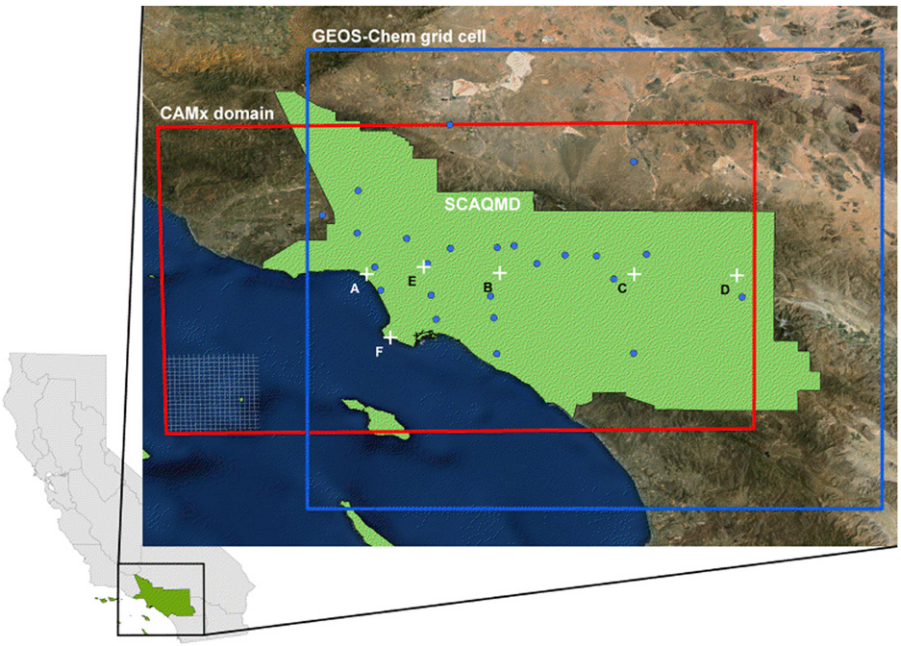

Fig. 1. Study region in Southern California. The green shaded region is the South Coast air quality Management District (SCAQMD). The blue line shows the outline of a single GEOS-Chem grid cell ($2 \times 2.5^\circ$). The red line shows the outline of the South Coast air basin (SoCAB), as employed in the CAMx modeling domain (9000 grid cells, 2×2 km^2 each; grid cells are illustrated in the lower left corner of the domain). Blue circles designate the 25 EPA monitors. White pluses and labels (a–f) correspond to the vertical profiles in Fig. 2 (a–f). (For interpretation of the references to color in this figure legend, the reader is referred to the web version of this article.)

Owing to interference from other reactive nitrogen species (NO_z), measurements of NO_x, and consequently NO_2, are often overestimated with this technique (US EPA, 1975; Steinbacher et al., 2007). The main interfering species are peroxyacetyl nitrate (PAN), nitric acid (HNO_3), and organic nitrates (Steinbacher et al., 2007). Dunlea et al. (2007) found that such interferences can account for up to 50% of afternoon NO_2 measured by chemiluminescence in Mexico City, but amount to less than 10% for more typical urban conditions (Boersma et al., 2009) where NO_x is a large portion of total reactive nitrogen (NO_y).

Lamsal et al. (2008) developed a method to estimate the NO_z interference for chemiluminescence analyzers based on modeled concentrations of the main interfering species. We apply this method here, using the CAMx model to estimate the interference and correct for it in the in situ measurements. The annual mean interference for all monitors in the SoCAB is 24% (inter-quartile range, 13–32%); annual mean interference is typically lower near major sources (see Fig. 2). Monitor interference is highest in the summer (seasonal mean interference for all monitors is 30%) and lowest in the winter (15%) owing to the longer NO_x lifetime in winter.

EPA monitoring data provide minimum detection limits for each of the monitors in the study region. However, a numeric estimate of the concentration is provided by EPA even when the value is below the nominal detection limit. Measurements below the monitor detection limit (which occurred during 14% of the measurements) were included unmodified in our analysis. Replacing those values with the detection limit value yielded almost no change in our results.

Comparisons below exclude data from one monitor, located upwind of the Los Angeles International Airport (LAX). For this monitor, the satellite and model pixels include the nearby airport, but the monitor, being upwind of the airport, likely is not strongly influenced by airport emissions.

2.4. Estimating surface concentrations

We use the GEOS-Chem and CAMx models to derive local NO_2 vertical profiles for the SoCAB. Fig. 1 shows the CAMx modeling domain (9000 grid cells, 150 × 240 km^2) and the GEOS-Chem grid cell (~220 × 230 km^2) that covers the study region. Differences in the spatial resolution of the models – grid cell area is four orders of magnitude larger for GEOS-Chem (~220 × 230 km^2) than for CAMx (2 × 2 km^2) – will result in differences in model output owing to nonlinearities in chemistry and dilution rates. GEOS-Chem assumes emissions from Los Angeles are instantly mixed throughout a large land area; CAMx makes physically similar assumptions but at much smaller spatial scales. The modeled NO_2 vertical profiles are influenced by the degree of mixing; differences in vertical mixing schemes employed by each model will also contribute to differences in model output. Our focus here is not on model–model comparison, but on assessing the information provided by the models for resolving within-urban air pollution gradients based on satellite data. Fig. 3 provides the NO_2 vertical profile from CAMx for several locations, and from GEOS-Chem.

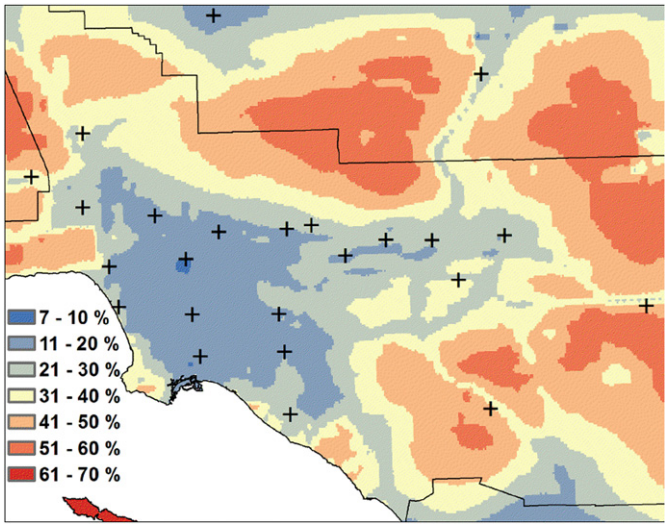

Fig. 2. Map of NO_z interference for chemiluminescence analyzers for the SoCAB as simulated by CAMx. Pluses indicate the 25 EPA monitors.

We infer surface NO_2 concentrations from the satellite observations by calculating a scaling factor (ratio of surface concentration to column abundance) for each satellite pixel. As our baseline approach we employ a constant scaling factor (1.0×10^{-15} ppb cm^2 $molec^{-1}$), calculated as the ratio of average in situ surface NO_2 to average OMI column abundance for coinciding measurements in the SoCAB. Because of the way the scale factor is constructed, using the EPA data, comparisons using this baseline approach are meaningful only in terms of correlation statistics and not for comparing absolute concentrations. We also obtain the temporally varying modeled scaling factors from the GEOS-Chem grid cell in the study region. For the CAMx scaling factors, the surface concentration reflects the model grid cell for each individual monitor, while the column abundance reflects an average over all model grid cells within each satellite pixel. The CAMx scaling factors assume a constant concentration above 2 km equal to the model boundary condition (0.02 ppb). Scaling factors from the CAMx model are, on average, larger than those from GEOS-Chem (median [inter-quartile range] in 10^{-16} ppb cm^2 $molec^{-1}$: 6.3 [4.9–8.1] for CAMx, 3.4 [2.9–3.9] for GEOS-Chem). Spatial variability, defined here as the coefficient-of-variability among monitoring-station locations, is lower for the CAMx scaling factors (21–38% for monthly mean values) compared to in situ and CAMx modeled surface concentrations (48–61%) and OMI column measurements (43–60%). Scaling factors from the CAMx model do not exhibit temporal patterns of note. GEOS-Chem scaling factors are lowest in the summer and highest in winter (median [units: 10^{-16} ppb cm^{-2} $molec^{-1}$]; 2.9 [summer], 4.3 [winter]). We apply these scaling factors to the OMI pixels to obtain daily surface NO_2 estimates for each monitor location. For each day we pair coinciding satellite and ground-level measurements ($N = 4138$).

3. Results

Data gaps were more prevalent for the OMI measurements than for EPA monitors (60% vs. 5%, respectively, of potentially available data from the OMI and EPA datasets). Because overlap at swath edges can potentially result in multiple OMI observations for a single monitor-day, only 47% (rather than 60%) of monitor-days lack corresponding satellite data (see Table S2). EPA monitors exhibit no statistical ($p < 0.001$) difference in NO_2 concentrations between days with or without satellite measurements, suggesting that excluding days with substantial cloud cover and/or haze does not bias our results. Summary statistics for each surface NO_2 estimation method are presented in Table 1. OMI-derived NO_2 and in situ measurements exhibit temporal correlation ($r = 0.4$–0.8) that is consistent with the findings of Lamsal et al. (2008) with the exception of one monitor ($r = 0.18$ [OMI] to 0.33 [CAMx]) located at the eastern edge of the study region. Pearson and Spearman correlation statistics ($r = 0.73$, $r_s = 0.77$; Fig. 4a, FigureS1a,b) and quartile-based kappa statistics ($\kappa = 0.37$, linear-weighted-$\kappa = 0.57$; Figure S1c,d) demonstrate a strong relationship between OMI column measurements and corrected EPA ground-level data (Figures S3–S5 provide pairwise scatter plots). This result indicates

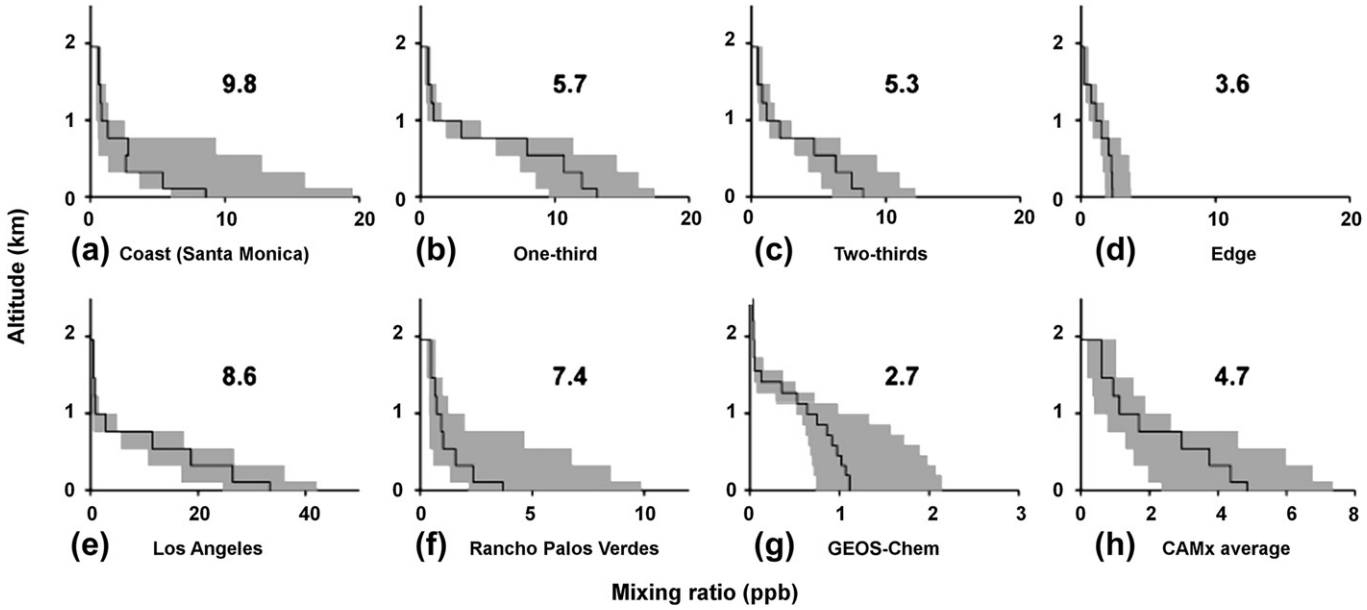

Fig. 3. Comparison of average NO_2 vertical profile estimates from (a–f) individual CAMx grid cells (see Fig. 1), (g) The GEOS-Chem grid cell, and (h) all CAMx cells within the GEOS-Chem grid cell (spatially averaged). Gray shading indicates the inter-quartile range. *X*-axis scales differ among plots. Number in each plot indicates surface-to-column ratio (units: 10^{-16} ppb cm^2 molec^{-1}) for that location.

that the within-urban spatial signature of ground-level NO_2 is well represented in the OMI data. A similar relationship (r = 0.71, r_s = 0.76, κ = 0.36, weighted-κ = 0.55; Fig. 4a, Figure S1a–d) is observed for OMI + GEOS-Chem surface estimates. Thus, employing the temporally varying GEOS-Chem-modeled scaling factors does not improve the ability of the satellite measurements to resolve fine-scale NO_2 gradients within a large urban area beyond the baseline approach using a constant scaling factor. The OMI + CAMx method exhibits a modest improvement over the baseline approach (r = 0.77, r_s = 0.83, κ = 0.44, weighted-κ = 0.64; Fig. 4a, Figure S1a–d). Correlation and kappa statistics do not demonstrate strong seasonal patterns (Figure S2a–d).

In addition to capturing spatial patterns of variability, for many air pollution exposure applications it is important for satellite-based methods to provide reliable absolute estimates of surface concentration. Fig. 5 shows that corrected measurements from EPA ground-level monitors are, on average, higher than the model and satellite-derived concentrations. The annual mean bias for satellite-based surface estimates is −50% and −13% for OMI + GEOS-Chem and OMI + CAMx methods respectively (Fig. 4b, Figure S1g). Both methods exhibit seasonal variation in bias, ranging from −37% in winter to −60% in summer for OMI + GEOS-Chem, and from <1% in spring to −22% in fall for OMI + CAMx (Figure S2g). In general, bias is lower in the winter/spring than in the summer/fall (Figure S2g); this pattern in the seasonal bias differs from the pattern reported by Lamsal et al. (2008, 2010).

The low average difference and bias for OMI + CAMx (Fig. 4b,c) imply that this method provides a reliable measure of fine-scale within-urban gradients of surface NO_2. To highlight this finding, Fig. 6 shows concentrations along a 160 km transect. A comparison of annual average estimates at each monitor over the study period reveals higher correlation and kappa statistics (Figure S1a–d) relative to the statistics for the ensemble of paired coincident measurements. Thus temporal averaging improves the spatial information content of the satellite-based estimates. Additional comparisons can be found in the online supplement (Tables S3–S9 and Figures S1–S5).

Table 1
Summary of 2005 annual average NO_2 estimates by method.

NO_2 estimate method	Mean (ppb)	St. Dev. (ppb)
EPA monitor	14.7	12.4
OMI + CAMx	10.1	8.3
CAMx only	11.9	8.6
OMI + GEOS-Chem	5.4	4.8

Another attribute for comparison is spatial and temporal coverage. OMI measurements are limited to the overpass time (~12:00–15:00 local time), whereas ground-based monitors provide 24-h coverage. Considering the region for which the CAMx domain and the GEOS-Chem grid cell overlap, each ground-based NO_2 monitor covers, on average, 1100 km^2 (i.e., total land area [27,000 km^2] divided by number of monitors [25]). On the other hand, the footprint of the OMI pixel at nadir is 310 km^2, and the average pixel size in the SoCAB over the study period is 550 km^2 (see Table 2). Considering gaps in the satellite data from clouds, data quality, and our imposed limits on pixel size, OMI's spatial coverage (calculated as the total land area divided by the average number of observations per day) is 730 km^2 per measurement – still more spatially precise than the ground monitors. While the (temporally averaged) satellite coverage is approximately geographically uniform, ground monitors are strategically placed near people. For example, spatial coverage of monitors in only the Los Angeles-Long Beach urban area (4400 km^2; 15 monitors) is 290 km^2 per measurement. For urban areas (UAs) in the continental US with at least one monitor, the average area per measurement is 460 km^2. However, only 28% of US UAs have any NO_2 monitors; for all UAs the spatial coverage is 690 km^2 per monitor measurement. Of the 448 US Census UAs in the contiguous US (total urban population: 191 million people), 20% (88 UAs, covering 29% of the urban population [56 million people]) have an average area per NO_2 monitor that is less than the average pixel size for OMI measurements employed here (550 km^2 measurement^{-1}); in the remaining 80% of UAs (71% of the urban population), OMI provides more spatial information than EPA monitoring stations. Further, OMI provides the same spatial coverage in non-urban areas, where ground-based monitors are sparse, as in UAs.

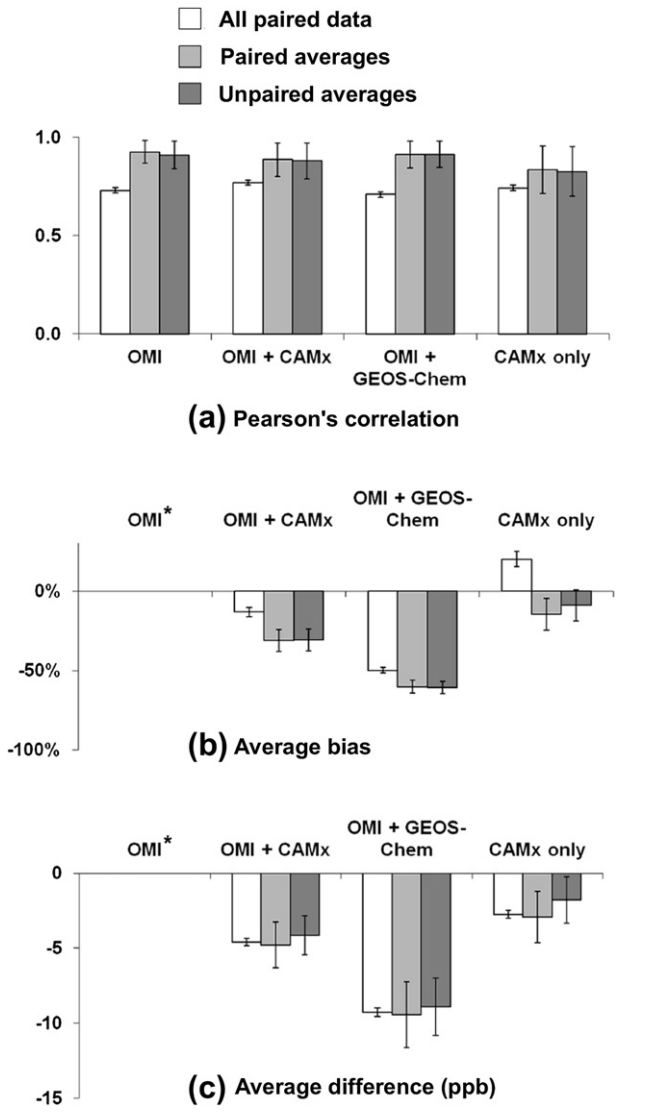

Fig. 4. Comparison of in situ measurements and model + OMI estimates of surface NO_2 concentrations. "Unpaired averages" is the annual average at each monitor for all available data ($n = 8666$ for EPA monitors; $n = 4575$ for OMI measurements). "Paired averages" employs the annual average at each monitor for days with coinciding satellite and EPA monitor measurements ($n = 25$ monitors). "All paired data" is the daily value at each monitor for days with coinciding OMI and EPA monitor measurements ($n = 4138$). Error bars indicate the 95% confidence interval. Values shown in this figure are also in Tables S3–S5. Certain comparisons, marked with an asterisk (*) are blank: Because of the way the scale factor is constructed (using the EPA data), comparisons using this baseline approach are meaningful for correlation statistics but not for comparing absolute concentrations.

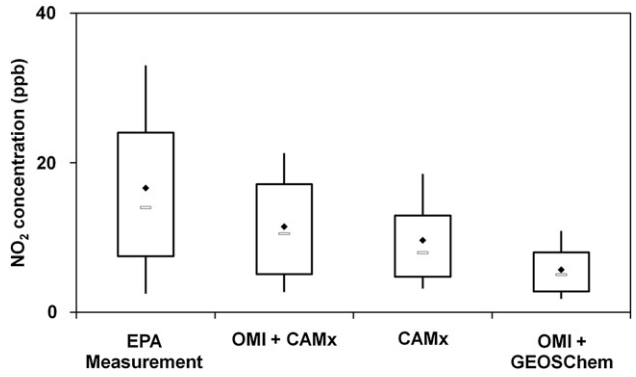

Fig. 5. Surface NO_2 concentration at monitor locations within the study region. Values shown are the mean (diamond), median (bar), 25th-75th percentiles (box), and 10th-90th percentiles (whiskers).

4. Discussion

Column measurements from the OMI sensor provide a robust measure of the ground-level NO_2 gradient within a large urban area ($r = 0.93$ for paired annual average data, compared to $r = 0.83$ for CAMx model estimates), suggesting that space-based NO_2 measurements could be a useful tool for exploring the spatial variability of urban air pollution exposure. An important finding is that OMI column measurements (without modeled scaling factors) outperform a well-developed urban-scale model (CAMx) at tracking the spatial variability of ground-level NO_2 in the SoCAB. The modeled local scaling factors used here provided little improvement in spatial correlation or kappa statistics relative to ground-based observations; however, scaling factors are necessary to estimate absolute surface concentrations from the satellite product. The correlations shown here between satellite-based NO_2 (OMI + CAMx, OMI + GEOS-Chem, and OMI columns) and corrected in situ measurements are generally higher than those previously reported. The OMI + GEOS-Chem surface estimates exhibit a larger negative bias than previously reported by Lamsal et al. (2008, 2010) for urban and suburban locations; this finding may suggest a regional difference in bias or differing performance between large and small urban locations. The OMI-based surface concentrations employing scaling factors from an urban-scale model (CAMx) provide robust estimates of absolute concentration (mean bias: −13%, versus 20% for CAMx-only estimates) and with complete spatial coverage for the SoCAB. Despite the coarse resolution of the OMI pixel relative to the CAMx urban-scale model, we find that the NO_2 signal from OMI can improve surface estimates from CAMx, illustrating the utility of satellite data in urban air-quality research, even for a region with a well-developed air dispersion model and detailed emission estimates. The OMI Standard Product is known to suffer from a seasonal bias; the amplitude of the seasonal bias found here is consistent with previous findings for urban locations, suggesting that the seasonal variation in bias may be less pronounced for urban than for rural locations (Lamsal et al., 2008, 2010).

Satellite-based observations measure average concentrations over a specific land area; ground-based observations represent concentrations at a single location. Even if both approaches were perfect, error-free records of concentrations, we would still expect differences between the two approaches owing to these differing spatial scales. Thus, the OMI versus ground-based comparisons presented here should be considered corroboration among approaches rather than a validation of either approach.

For applications such as environmental epidemiology, or understanding broad compliance with ambient standards, the spatial precision provided by the satellite data may be of particular value. OMI observations provide good spatial coverage that is comparable to (and in most UAs, better than) current ground-level monitoring networks in urban areas, and better than the current network in rural areas. Within-urban gradients in ground-level NO_2 observed from the OMI sensor thus provide a useful dataset for exploring epidemiological impacts of urban air pollution. These measurements can also provide high-quality air pollution estimates where monitoring data are lacking, or can be incorporated into large-scale land use regression (LUR) models; LUR models can be 1–2 orders of magnitude more spatially precise than satellite data alone (e..g, ~10–20 km [satellite], ~0.1 km [LUR]) (Hystad et al., 2011; Novotny et al., 2011).

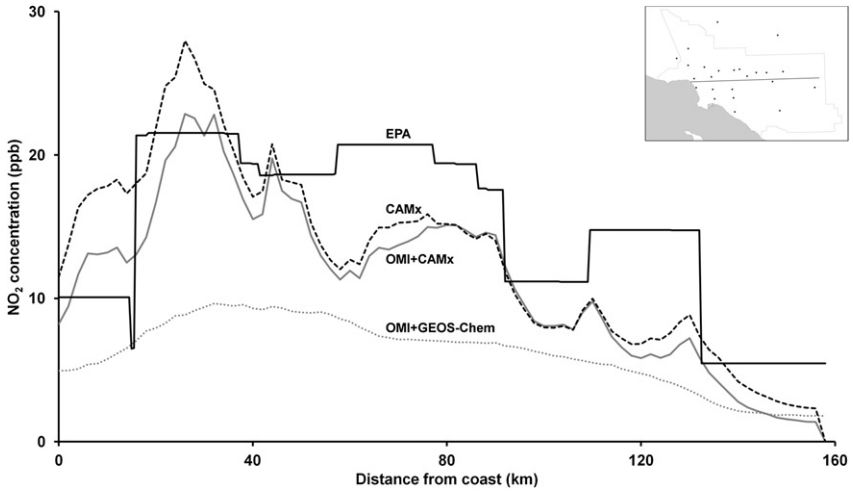

Fig. 6. Estimated annual average surface NO_2 concentrations along the 160-km transect shown inset. EPA values for this figure correspond to those for the nearest monitor; the inset map also shows monitor locations.

Table 2
Spatial coverage for OMI vs. ground-level monitors.

		Mean area (km^2) per measurement
OMI pixel size	at nadir	310
	average for SoCAB	550
	inter-quartile range for SoCAB	360–650
Land area per OMI observation[a]	average for SoCAB	730
	inter-quartile range for SoCAB	450–2400
Land area per EPA monitor[b]	average for SoCAB	1100
	average for Los Angeles urban area	290
	average for all US urban areas[c]	690
	average for US urban areas with at least one monitor[c]	460
	inter-quartile range for US urban areas with at least one monitor[c]	160–670
	average for continental US excluding urban areas	45,000

[a] For the 279 days with satellite observations. Calculated as the ratio of land area in the SoCAB to the average number of OMI pixels per day. This metric accounts for gaps in satellite data from cloud cover and our own imposed limits on pixel size.
[b] Calculated as the ratio of land area in the SoCAB to the number of EPA monitors.
[c] The year-2000 US Census lists 448 Urban Areas in the continental US; of those, 29% (128 Urban Areas) have at least one monitor.

The use of satellite observations to estimate surface concentrations is not limited to NO_2. Past studies have shown a close relationship between remotely sensed aerosol optical depth (AOD) and ground-level particulate matter concentrations (Martin, 2008). More recently, methods have been developed to infer surface PM_{10} (diameter < 10 μm) and $PM_{2.5}$ (diameter < 2.5 μm) from satellite observations of AOD (Brauer et al., 2012; Liu et al., 2004, 2005, 2007b; van Donkelaar et al., 2006, 2010; Weber et al., 2010). Satellite-based AOD measurements have also been incorporated into temporally and spatially resolved LUR models for $PM_{2.5}$ in the Northeast United States (Kloog et al., 2011, 2012a,b). The correlation statistics we report in this work for ground-level NO_2 are similar to those found for regional- and national-scale comparisons between satellite-based and in situ $PM_{2.5}$ estimates (Liu et al., 2004, 2005; van Donkelaar et al., 2006, 2010). A study that evaluated satellite-based estimates of $PM_{2.5}$ for a single urban area (St. Louis, MO) reported similar correlation statistics ($r = 0.71$–0.79) and bias (-12% to -18%) as our findings for ground-level NO_2 (Liu et al., 2007a).

We have shown for the SoCAB that OMI provides a reliable measure of spatial variability of ground-level NO_2 within a large urban area, and an accurate measure of ground-level NO_2 concentrations when combined with an urban-scale model. Results may differ among urban areas; for example, resolving urban-scale spatial gradients may be more difficult for small urban areas. While use of an urban-scale model is not practical for most urban areas (robust urban-scale models may or may not have been developed for any one specific urban area), we find that the OMI column measurements can be a useful proxy for ground-level variability in NO_2 concentrations. Our findings also suggest that OMI measurements may be a useful tool for exploring NO_2 variability between urban locations, particularly for urban areas with few or no ground-based monitors. Recent work has shown that OMI slant column measurements using the super-zoom mode (13×3 km^2 resolution) can capture spatial variability in NO_2 at even finer scales than is achievable with OMI's operational footprint (13×24 km^2 resolution) (Valin et al., 2011b). The Sentinel-5 Precursor mission (expected launch 2015; http://esamultimedia.esa.int/docs/S5-prec_Data_Sheet.pdf) will offer improved spatial resolution ($\sim 7 \times 7$ km^2 at nadir) and global daily coverage. Geo-stationary measurements from TEMPO (http://www.nasa.gov/home/hqnews/2012/nov/HQ_12-390_TEMPO_Instrument.html) and GEO-CAPE (http://geo-cape.larc.nasa.gov/) are also expected to provide improved spatial resolution ($\sim 4 \times 4$ km^2 resolution, or $\sim 20 \times$ better than the OMI nadir pixel) and near hourly coverage. Our findings here emphasize the power of such measurements for quantifying spatial (as well as temporal) gradients in ground-level NO_2 within urban areas, particularly those areas with limited in situ monitors.

Acknowledgments

This work was supported by NSF-Division of Chemical, Bioengineering, Environmental, and Transport Systems (CBET) (grant 0853467). We acknowledge the NASA GES DISC for the dissemination of OMI data, and the US EPA AQS Data Mart for the dissemination of EPA monitor data.

Appendix A. Supplementary data

Supplementary data related to this article can be found at http://dx.doi.org/10.1016/j.atmosenv.2012.11.046.

References

Acarreta, J.R., De Haan, J.F., Stammes, P., 2004. Cloud pressure retrieval using the O_2-O_2 absorption band at 477 nm. Journal of Geophysical Research 109 (D05204). http://dx.doi.org/10.1029/2003JD003915.

Beelen, R., Hoek, G., van den Brandt, P.A., Goldbohm, R.A., Fischer, P., Schouten, L.J., Jerrett, M., Hughes, E., Armstrong, B., Brunekreef, B., 2008. Long-term effects of traffic-related air pollution on mortality in a Dutch cohort (NLCS-AIR study). Environmental Health Perspectives 116 (2), 196–202.

Blond, N., Boersma, K.F., Eskes, H.J., van der A, R.J., Van Roozendael, M., De Smedt, I., Bergametti, G., Vautard, R., 2007. Intercomparison of SCIAMACHY nitrogen dioxide observations, in situ measurements and air quality modeling over Western Europe. Journal of Geophysical Research 112 (D10311). http://dx.doi.org/10.1029/2006JD007277.

Boersma, K.F., Bucsela, E., Brinksma, E.J., Gleason, J.F., 2002. NO_2. In: Chance, K. (Ed.), OMI Algorithm Theoretical Basis Document, OMI Trace Gas Algorithms, ATB-OMI-04, Version 2.0, vol. 4. KNMI, De Bilt, The Netherlands, pp. 13–36.

Boersma, K.F., Eskes, H.J., Brinksma, E.J., 2004. Error analysis for tropospheric NO_2 retrieval from space. Journal of Geophysical Research 109 (D04311). http://dx.doi.org/10.1029/2003JD003962.

Boersma, K.F., Jacob, D.J., Trainic, M., Rudich, Y., De Smedt, I., Dirksen, R., Eskes, H.J., 2009. Validation of urban NO_2 concentrations and their diurnal and seasonal variations observed from the SCIAMACHY and OMI sensors using in situ surface measurements in Israeli cities. Atmospheric Chemistry and Physics 9. http://dx.doi.org/10.5194/acp-9-3867-2009.

Brauer, M., Lencar, C., Tamburic, L., Koehoorn, M., Demers, P., Karr, C., 2008. A cohort study of traffic-related air pollution impacts on birth outcomes. Environmental Health Perspectives 116 (5), 680–686.

Brauer, M., Amann, M., Burnett, R.T., Cohen, A., Dentener, F., Ezzati, M., Henderson, S.B., Krzyzanowski, M., Martin, R.V., Van Dingenen, R., van Donkelaar, A., Thurston, G.D., 2012. Exposure assessment for estimation of the global burden of disease attributable to outdoor air pollution. Environmental Science and Technology 46 (12), 652–660.

Burrows, J.P., Weber, M., Buchwitz, M., Rozanov, V., Ladstätter-Weißenmayer, A., Richter, A., DeBeek, R., Hoogen, R., Bramstedt, K., Eichmann, K., Eisinger, M., 1999. The Global Ozone Monitoring Experiment (GOME): mission concept and first scientific results. Journal of the Atmospheric Sciences 56 (2), 151–175.

Bucsela, E.J., Celarier, E.A., Wenig, M.O., Gleason, J.F., Veefkind, J.P., Boersma, K.F., Brinksma, E.J., 2006. Algorithm for NO_2 vertical column retrieval from the Ozone Monitoring Instrument. IEEE Transactions on Geoscience and Remote Sensing 44 (5), 1245–1258.

Castellsague, J., Sunyer, J., Saez, M., Anto, J.M., 1995. Short-term association between air pollution and emergency room visits for asthma in Barcelona. Thorax 50 (10), 1051–1056.

Celarier, E.A., Brinksma, E.J., Gleason, J.F., Veefkind, J.P., Cede, A., Herman, J.R., Ionov, D., Goutail, F., Pommereau, J.P., Lambert, J.C., van Roozendael, M., Pinardi, G., Wittrock, F., Schönhardt, A., Richter, A., Ibrahim, O.W., Wagner, T., Bojkov, B., Mount, G., Spinei, E., Chen, C.M., Pongetti, T.J., Sander, S.P., Bucsela, E.J., Wenig, M.O., Swart, D.P.J., Volten, H., Kroon, M., Levelt, P.F., 2008. Validation of Ozone Monitoring Instrument nitrogen dioxide columns. Journal of Geophysical Research 113 (D15S15). http://dx.doi.org/10.1029/2007JD008908.

Duncan, B.N., Yoshida, Y., Olson, J.R., Sillman, S., Martin, R.V., Lamsal, L., Hu, Y., Pickering, K.E., Retscher, C., Allen, D.J., Crawford, J.H., 2010. Application of OMI observations to a space-based indicator of NO_x and VOC controls on surface ozone formation. Atmospheric Environment 44 (18), 2213–2223.

Dunlea, E.J., Herndon, S.C., Nelson, D.D., Volkamer, R.M., San Martini, F., Sheehy, P.M., Zahniser, M.S., Shorter, J.H., Wormhoudt, J.C., Lamb, B.K., Allwine, E.J., Gaffney, J.S., Marley, N.A., Grutter, M., Marquez, C., Blanco, S., Cardenas, B., Retama, A., Ramos Villegas, C.R., Kolb, C.E., Molina, L.T., Molina, M.J., 2007. Evaluation of nitrogen dioxide chemiluminescence monitors in a polluted urban environment. Atmospheric Chemistry and Physics 7. http://dx.doi.org/10.5194/acp-7-2691-2007.

Filleul, L., Rondeau, V., Vandentorren, S., Le Moual, N., Cantagrel, A., Annesi-Maesano, I., Charpin, D., Declercq, C., Neukirch, F., Paris, C., Vervloet, D., Brochard, P., Tessier, J.F., Kauffmann, F., Baldi, I., 2005. Twenty five year mortality and air pollution: results from the French PAARC survey. Occupational and Environmental Medicine 62 (7), 453–460.

Gauderman, W.J., Avol, E., Lurmann, F., Kuenzli, N., Gilliland, F., Peters, J., McConnell, R., 2005. Childhood asthma and exposure to traffic and nitrogen dioxide. Epidemiology 16 (6), 737–743.

Ghude, S.D., Kulkarni, P.S., Kulkarni, S.H., Fadnavis, S., van der A, R.J., 2011. Temporal variation of urban NO_x concentration in India during the past decade as observed from space. International Journal of Remote Sensing 32 (3), 849–861.

Hoek, G., Beelen, R., de Hoogh, K., Vienneau, D., Gulliver, J., Fischer, P., Briggs, D., 2008. A review of land-use regression models to assess spatial variation of outdoor air pollution. Atmospheric Environment 42 (33), 7561–7578.

Hudman, R.C., Jacob, D.J., Turquety, S., Leibensperger, E.M., Murray, L.T., Wu, S., Gilliland, A.B., Avery, M., Bertram, T.H., Brune, W., Cohen, R.C., Dibb, J.E., Flocke, F.M., Fried, A., Holloway, J., Neuman, J.A., Orville, R., Perring, A., Ren, X., Sachse, G.W., Singh, H.B., Swanson, A., Wooldridge, P.J., 2007. Surface and lightning sources of nitrogen oxides over the United States: magnitudes, chemical evolution, and outflow. Journal of Geophysical Research 112 (D12S05). http://dx.doi.org/10.1029/2006JD007912.

Hudman, R.C., Murray, L.T., Jacob, D.J., Millet, D.B., Turguety, S., Wu, S., Blake, D.R., Goldstein, A.H., Holloway, J., Sachse, G.W., 2008. Biogenic vs. anthropogenic sources of CO over the United States. Geophysical Research Letters 34 (L04801). http://dx.doi.org/10.1029/2007GL032393.

Hystad, P., Setton, E., Cervantes, A., Poplawski, K., Deschenes, S., Brauer, M., van Donkelaar, A., Lamsal, L., Martin, R., Jerret, M., Demers, P., 2011. Creating national air pollution models for population exposure assessment in Canada. Environmental Health Perspectives 119 (8), 1123–1129.

Kim, J.J., Smorodinsky, S., Lipsett, M., Singer, B.C., Hodgson, A.T., Ostro, B., 2004. Traffic-related air pollution near busy roads: the East Bay Children's Respiratory Health Study. American Journal of Respiratory and Critical Care Medicine 170 (5), 520–526.

Kloog, I., Koutrakis, P., Coull, B.A., Joo Lee, H., Schwartz, J.D., 2011. Assessing temporally and spatially resolved PM2.5 exposures for epidemiological studies using satellite aerosol optical depth measurements. Atmospheric Environment 45 (35), 6267–6275.

Kloog, I., Coull, B.A., Zanobetti, A., Koutrakis, P., Schwartz, J.D., 2012a. Acute and chronic effects of particles on hospital admissions in New-England. PLoS ONE 7 (4), e34664. http://dx.doi.org/10.1371/journal.pone.0034664.

Kloog, I., Nordio, F., Coull, B.A., Schwartz, J.D., 2012b. Incorporating local land use regression and satellite aerosol optical depth in a hybrid model of spatiotemporal PM2.5 exposures in the Mid-Atlantic states. Environmental Science and Technology 46 (21), 11913–11921.

Kramer, L.J., Leigh, R.J., Remedios, J.J., Monks, P.S., 2008. Comparison of OMI and ground-based in situ and MAX-DOAS measurements of tropospheric nitrogen dioxide in an urban area. Journal of Geophysical Research 113 (D16S39). http://dx.doi.org/10.1029/2007JD009168.

Lamsal, L.N., Martin, R.V., van Donkelaar, A., Steinbacher, M., Celarier, E.A., Bucsela, E., Dunlea, E.J., Pinto, J.P., 2008. Ground-level nitrogen dioxide concentrations inferred from the satellite-borne Ozone Monitoring Instrument. Journal of Geophysical Research 113 (D16308). http://dx.doi.org/10.1029/2007JD009235.

Lamsal, L.N., Martin, R.V., van Donkelaar, A., Celarier, E.A., Bucsela, E.J., Boersma, K.F., Dirksen, R., Luo, C., Wang, Y., 2010. Indirect validation of tropospheric nitrogen dioxide retrieved from the OMI satellite instrument: insight into the seasonal variation of nitrogen oxides at northern midlatitudes. Journal of Geophysical Research 115 (D05302). http://dx.doi.org/10.1029/2009JD013351.

Levelt, P.F., van den Oord, G.H.J., Dobber, M.R., Mälkki, A., Visser, H., de Vries, J., Stammes, P., Lundell, J.O.V., Saari, H., 2006. The Ozone Monitoring Instrument. IEEE Transactions on Geoscience and Remote Sensing 44 (5), 1093–1101.

Liang, J., Horowitz, L.W., Jacob, D.J., Wang, Y., Fiore, A.M., Logan, J.A., Gardner, G.M., Munger, J.W., 1998. Seasonal budgets of reactive nitrogen species and ozone over the United States, and export fluxes to the global atmosphere. Journal of Geophysical Research 103 (D11). http://dx.doi.org/10.1029/97JD03126.

Lin, J.-T., McElroy, M.B., 2010. Impacts of boundary layer mixing on pollutant vertical profiles in the lower troposphere: implications to satellite remote sensing. Atmospheric Environment 44 (14), 1726–1739.

Liu, Y., Park, R.J., Jacob, D.J., Li, Q., Kilaru, V., Sarnat, J.A., 2004. Mapping annual mean ground-level PM2.5 concentrations using Multiangle Imaging Spectroradiometer aerosol optical thickness over the contiguous United States. Journal of Geophysical Research 109 (D22206). http://dx.doi.org/10.1029/2004JD005025.

Liu, Y., Sarnat, J.A., Kilaru, V., Jacob, D.J., Koutrakis, P., 2005. Estimating ground-level $PM_{2.5}$ in the Eastern United States using satellite remote sensing. Environmental Science and Technology 39 (9), 3269–3278.

Liu, Y., Franklin, M., Kahn, R., Koutrakis, P., 2007a. Using aerosol optical thickness to predict ground-level $PM_{2.5}$ concentrations in the St. Louis area: a comparison between MISR and MODIS. Remote Sensing of Environment 107 (1–2), 33–44.

Liu, Y., Koutrakis, P., Kahn, R., 2007b. Estimating fine particulate matter component concentrations and size distributions using satellite-retrieved fractional aerosol optical depth: part 1 – method development. Journal of the Air and Waste Management Association 57 (11), 1351–1359.

Madsen, C., Gehring, U., Eldevik Håberg, S., Nafstad, P., Meliefste, K., Nystad, W., Lødrup Carlsen, K.C., Brunekreef, B., 2011. Comparison of land-use regression models for predicting spatial NOx contrasts over a three year period in Oslo, Norway. Atmospheric Environment 45 (21), 3576–3583.

Marshall, J.D., Nethery, E., Brauer, M., 2008. Within-urban variability in ambient air pollution: comparison of estimation methods. Atmospheric Environment 42 (6), 1359–1369.

Martin, R.V., 2008. Satellite remote sensing of surface air quality. Atmospheric Environment 42 (34), 7823–7843.

Martin, R.V., Chance, K., Jacob, D.J., Kurosu, T.P., Spurr, R.J.D., Bucsela, E., Gleason, J.F., Palmer, P.I., Bey, I., Fiore, A.M., Li, Q., Yantosca, R.M., Koelemeijer, R.B.A., 2002. An improved retrieval of tropospheric nitrogen dioxide from GOME. Journal of Geophysical Research 107 (4437). http://dx.doi.org/10.1029/2001JD001027.

Mathers, C.D., Stevens, G., Mascarenhas, M., 2009. Global Health Risks: Mortality and Burden of Disease Attributable to Selected Major Risks. World Health Organization, Geneva, Switzerland.

Meng, Z.Y., Xu, X.B., Wang, T., Zhang, X.Y., Yu, X.L., Wang, S.F., Lin, W.L., Chen, Y.Z., Jiang, Y.A., An, X.Q., 2010. Ambient sulfur dioxide, nitrogen dioxide, and ammonia at ten background and rural sites in China during 2007–2008. Atmospheric Environment 44 (21–22), 2625–2631.

Novotny, E.V., Bechle, M.J., Millet, D.B., Marshall, J.D., 2011. National satellite-based land-use regression: NO_2 in the United States. Environmental Science and Technology 45 (10), 4407–4414.

Ordoñez, C., Richter, A., Steinbacher, M., Zellweger, C., Nüß, H., Burrows, J.P., Prévôt, A.S.H., 2006. Comparison of 7 years of satellite-borne and ground-based tropospheric NO_2 measurements around Milan, Italy. Journal of Geophysical Research 111 (D05310). http://dx.doi.org/10.1029/2005JD006305.

Ospital, J., Cassmassi, J., Chico, T., 2008. Multiple Air Toxics Exposure Study in the South Coast Air Basin (MATES III). South Coast Air Quality Management District, Diamond Bar, CA.

Petritoli, A., Bonasoni, P., Giovanelli, G., Ravegnani, F., Kostadinov, I., Bortoli, D., Weiss, A., Schaub, D., Richter, A., Fortezza, F., 2004. First comparison between ground-based and satellite-borne measurements of tropospheric nitrogen dioxide in the Po basin. Journal of Geophysical Research 109 (D15307). http://dx.doi.org/10.1029/2004JD004547.

Russell, A.R., Valin, L.C., Bucsela, E.J., Wenig, M.O., Cohen, R.C., 2010. Space-based constraints on spatial and temporal patterns of NO_x emissions in California, 2005–2008. Environmental Science and Technology 44 (9), 3608–3615.

Russell, A.R., Perring, A.E., Valin, L.C., Bucsela, E., Browne, E.C., Min, K.-E., Wooldridge, P.J., Cohen, R.C., 2011. A high spatial resolution retrieval of NO_2 column densities from OMI: method and evaluation. Atmospheric Chemistry and Physics 11, 8543–8554.

Schoeberl, M.R., Douglass, A.R., Hilsenrath, E., Bhartia, P.K., Beer, R., Waters, J.W., Gunson, M.R., Froidevaux, L., Gille, J.C., Barnett, J.J., Levelt, P.F., DeCola, P., 2006. Overview of the EOS aura mission. IEEE Transactions on Geoscience and Remote Sensing 44 (5), 1066–1074.

South Coast Air Quality Management District, 2007. 2007 Air Quality Management Plan. South Coast Air Quality Management District, Diamond Bar, CA.

Steinbacher, M., Zellweger, C., Schwarzenbach, B., Bugmann, S., Buchmann, B., Ordoñez, C., Prévôt, A.S.H., Hueglin, C., 2007. Nitrogen oxide measurements at rural sites in Switzerland: bias of conventional measurement techniques. Journal of Geophysical Research 112 (D11307). http://dx.doi.org/10.1029/2006JD007971.

US Environmental Protection Agency, 1975. Technical Assistance Document for the Chemiluminescence Measurement of Nitrogen Dioxide. US Environmental Protection Agency, Research Triangle Park, NC.

US Environmental Protection Agency, Office of Air Quality Planning and Standards, 2008. National Air Quality and Emissions Trend Report. US Environmental Protection Agency, Research Triangle Park, NC.

Valin, L.C., Russell, A.R., Hudman, R.C., Cohen, R.C., 2011a. Effects of model resolution on the interpretation of satellite NO_2 observations. Atmospheric Chemistry and Phsyics 11, 11647–11655.

Valin, L.C., Russell, A.R., Bucsela, E.J., Veefkind, J.P., Cohen, R.C., 2011b. Observation of slant column NO_2 using the super-zoom mode of AURA-OMI. Atmospheric Measurement Techniques 4, 1929–1935.

van Donkelaar, A., Martin, R.V., Park, R.J., 2006. Estimating ground-level $PM_{2.5}$ using aerosol optical depth determined from satellite remote sensing. Journal of Geophysical Research 111 (D21201). http://dx.doi.org/10.1029/2005JD006996.

van Donkellar, A., Martin, R.V., Brauer, M., Kahn, R., Levy, R., Verduzco, C., Villeneuve, P.J., 2010. Global estimates of ambient fine particulate matter concentrations from satellite-based aerosol optical depth: development and application. Environmental Health Perspectives 118 (6), 847–855.

Weber, S.A., Engel-Cox, J.A., Hoff, R.M., Prados, A.I., Zhang, H., 2010. An improved method for estimating surface fine particle concentrations using seasonally adjusted satellite aerosol optical depth. Journal of the Air and Waste Management Association 60 (5), 574–585.

Supplemental Online Materials

Remote sensing of exposure to NO_2: satellite versus in situ measurement in a large urban area

Matthew J. Bechle[a], Dylan B. Millet[a, b], Julian D. Marshall[a, *]

[a] *Department of Civil Engineering, University of Minnesota, Minneapolis, MN 55455*

[b] *Department of Soil, Water, and Climate, University of Minnesota, Minneapolis, MN 55455*

[*]Corresponding author. Phone: (612) 625-3297; fax: (612) 626-7750; e-mail: julian@umn.edu.

Table S1: Summary of articles comparing satellite and ground-level measurements of NO_2

Publication	Satellite instrument	Location & Time	Summary
Blond et al., 2007.	SCIAMACHY	Western Europe; 2003	Compared annual average surface NO_2 measurements with SCIAMACHY tropospheric NO_2 and found low spatial correlation (r = 0.43, n = 176) when considering all monitors (urban, suburban, and rural), agreement improves when considering only rural surface monitors (r = 0.90, n = 29).
Boersma et al., 2009.	OMI & SCIAMACHY	Six Isreali cities (Carmiel, Afula, Modiin, Rehovot, Beit Shemesh, and Beer Sheva); 2006	Estimated boundary-layer NO_2 from six surface NO_2 monitors in Isreali cities using model NO_2 profiles from GEOS-Chem. Found good spatio-temporal correlation between estimated boundary-layer NO_2 and tropospheric NO_2 columns from OMI (r = 0.63) and SCIAMACHY (r = 0.46-0.54).
Duncan et al., 2010.	OMI	Continental US; Summer (June-August) 2005-2007	Calculated surface ozone-precursor sensitivity as the ratio of OMI column formaldehyde to NO_2 and gridded to 0.25° grid. The calculated ozone-precursor sensitivity was found to be broadly consistent with results from in situ and modeling studies, including those in the SoCAB.
Ghude et al., 2011.	OMI	Delhi, India; March 1996–December 2007	Compared 2-years of daily average surface NO_x concentrations at a monitor located in Delhi, India with OMI tropospheric column NO_2 averaged over a 1° × 1° grid cell centered at Delhi (r = 0.45, n = 522).
Kramer et al., 2008.	OMI	Leicester, England; 2005-2006	Compared OMI tropospheric NO_2 with the spatial average of four background surface NO_2 monitors (r = 0.43). Developed an improved surface estimate by including measurements from a nearby rural monitor and performing an area-weighted concentration to account for the fraction of the urban area in the satellite field-of-view, the improved estimate exhibited an improved temporal correlation (r = 0.83 & r = 0.64 for spring and summer respectively).
Lamsal et al., 2008.	OMI	US and Canada; 2005	Inferred ground-level NO_2 concentrations from OMI tropospheric NO_2 by applying modeled scaling factors derived from GEOS-Chem. Compared OMI-based surface NO_2 with corrected in situ surface NO_2 concentrations (bias -11%-36%), found good temporal correlation (up to r = 0.86) with highest correlations in more polluted areas.

Lamsal et al., 2010.	OMI	Southeast US; 2005-2006	Calculated ground-level estimates of NO_2 derived from OMI tropospheric columns using modeled surface-to-column ratios from GEOS-Chem. Compared OMI-based surface NO_2 with in situ measurements at rural locations and found broadly consistent seasonal variation. Bias for the Standard OMI product (27%-43%) was found to be higher than for the DOMINO product (21%-33%), with the highest bias occurring in summer months (67%-74%).
Meng et al., 2010.	OMI	China; 2007-2008	Calculated monthly average OMI tropospheric NO_2 (using the 0.25° × 0.25° gridded product) for regional background and rural monitoring sites. Monthly mean OMI and in situ ground-level measurementsexhibit significant temporal correlation for six of the ten monitors (r = 0.47 – 0.75).
Ordoñez et al., 2006.	GOME	Lombardy region of northern Italy; 1996-2002	Compared tropospheric GOME NO_2 with 99 ground-level in situ NO_2 monitors corrected for NO_x interference, found good spatio-temporal correlation (r = 0.58 & r = 0.76 for winter-autumn and spring-summer respectively). Estimated tropospheric NO_2 from the in situ monitors using seasonal average scaling factors derived from modeled daily NO_2 vertical profiles from MOZART. A weighted-orthogonal regression was conducted for each concentration quintile and found good spatio-temporal correlation (r = 0.67 – 0.80) with the best fit for slightly- and average-polluted monitors (2^{nd} and 3^{rd} quintile).
Petritoli et al., 2004.	GOME	Po valley in northern Italy; 2000-2001	Found that annual cycle in surface NO_2 and some pollution episodes measured by a background monitor are well reproduced by GOME tropospheric NO_2 measurements. Estimated tropspheric column NO_2 from surface measurements assuming a well-mixed PBL, monthly correlations between estimated tropospheric NO_2 and GOME NO_2 show good agreement (r > 0.84 for each month).
Russell et al., 2010.	OMI	California (Sacremento County, San Francisco Bay Area, San Joaquin Valley, and the South Coast Air Basin); Summer (June-August) 2005-2008	Calculated monthly average OMI tropospheric NO_2 binned to 0.025° grid for California. The spatial average of OMI tropospheric NO_2 and in situ ground-level measurements are calculated for four regions in California. Day-of-week and annual trends for OMI and ground-based measurements exhibit similar patterns.

Table S2: Summary of removed and missing data

	All available data	Monitoring days
Total possible from OMI	14772	8564
% removed owing to our limitations on pixel size	33%	17%
% removed owing to cloud cover	19%	24%
% removed owing to flags and missing data	8%	7%
Total possible from EPA	--	9125
% removed owing to missing data	--	5%
Total coinciding	--	4258
Total Used	--	4138

Table S3: Comparison of model+OMI estimates of surface NO_2 with in situ measurements (paired daily data)

Statistic	OMI[a]	OMI + CAMx	OMI + GEOS-Chem	CAMx only
Avg. difference (ppb)	N/A	-5.60	-9.29	-2.75
Avg. absolute difference (ppb)	N/A	6.24	9.51	5.74
Avg. bias (%)	N/A	-13%	-50%	20%
Avg. absolute bias (%)	N/A	50%	63%	60%
Pearson's correlation	0.73	0.77	0.71	0.74
Spearman's correlation	0.77	0.83	0.76	0.82
Kappa	0.37	0.44	0.36	0.44
Weighted-Kappa	0.57	0.64	0.55	0.63

[a]Assuming a constant scale factor of 1.0×10^{-15} ppb cm^2 $molec^{-1}$. Because of the way the scale factor is constructed (using the EPA data), comparisons using this baseline approach are meaningful only in terms of correlation statistics and not for comparing absolute concentrations.

Table S4: Comparison of model+OMI estimates of surface NO_2 with in situ measurements (paired annual average data)

Statistic	OMI[a]	OMI + CAMx	OMI + GEOS-Chem	CAMx only
Avg. difference (ppb)	N/A	-4.80	-9.45	-2.94
Avg. absolute difference (ppb)	N/A	5.03	9.45	4.22
Avg. bias (%)	N/A	-31%	-60%	-15%
Avg. absolute bias (%)	N/A	33%	60%	26%
Pearson's correlation	0.93	0.89	0.91	0.83
Spearman's correlation	0.91	0.94	0.91	0.93
Kappa	0.63	0.68	0.63	0.68
Weighted-Kappa	0.75	0.81	0.75	0.81

[a]Assuming a constant scale factor of 1.0×10^{-15} ppb cm^2 $molec^{-1}$. Because of the way the scale factor is constructed (using the EPA data), comparisons using this baseline approach are meaningful only in terms of correlation statistics and not for comparing absolute concentrations.

Table S5: Comparison of model+OMI estimates of surface NO_2 with in situ measurements (unpaired summer average data)

Statistic	OMI[a]	OMI + CAMx	OMI + GEOS-Chem	CAMx only
Avg. difference (ppb)	N/A	-4.17	-8.91	-1.79
Avg. absolute difference (ppb)	N/A	4.42	8.91	3.46
Avg. bias (%)	N/A	-31%	-61%	-9%
Avg. absolute bias (%)	N/A	32%	61%	23%
Pearson's correlation	0.91	0.88	0.91	0.83
Spearman's correlation	0.87	0.93	0.86	0.91
Kappa	0.63	0.57	0.63	0.63
Weighted-Kappa	0.75	0.75	0.75	0.75

[a]Assuming a constant scale factor of 1.0×10^{-15} ppb cm^2 $molec^{-1}$. Because of the way the scale factor is constructed (using the EPA data), comparisons using this baseline approach are meaningful only in terms of correlation statistics and not for comparing absolute concentrations.

Table S6: Comparison of model+OMI estimates of surface NO_2 with in situ measurements (spring data, n=936)

Statistic	OMI[a]	OMI + CAMx	OMI + GEOS-Chem	CAMx only
Avg. difference (ppb)	N/A	-2.80	-7.71	-2.63
Avg. absolute difference (ppb)	N/A	5.30	8.02	5.47
Avg. bias (%)	N/A	0.5%	-40%	32%
Avg. absolute bias (%)	N/A	51%	59%	71%
Pearson's correlation	0.69	0.75	0.72	0.73
Spearman's correlation	0.77	0.85	0.77	0.81
Kappa	0.38	0.46	0.35	0.44
Weighted-Kappa	0.58	0.64	0.55	0.61

[a]Assuming a constant scale factor of 1.0×10^{-15} ppb cm^2 $molec^{-1}$. Because of the way the scale factor is constructed (using the EPA data), comparisons using this baseline approach are meaningful only in terms of correlation statistics and not for comparing absolute concentrations.

Table S7: Comparison of model+OMI estimates of surface NO_2 with in situ measurements (summer data, n=1344)

Statistic	OMI[a]	OMI + CAMx	OMI + GEOS-Chem	CAMx only
Avg. difference (ppb)	N/A	-4.15	-9.05	-2.36
Avg. absolute difference (ppb)	N/A	5.33	9.12	4.71
Avg. bias (%)	N/A	-13%	-60%	16%
Avg. absolute bias (%)	N/A	50%	68%	56%
Pearson's correlation	0.69	0.75	0.64	0.75
Spearman's correlation	0.74	0.82	0.71	0.82
Kappa	0.32	0.41	0.30	0.44
Weighted-Kappa	0.53	0.62	0.51	0.62

[a]Assuming a constant scale factor of 1.0×10^{-15} ppb cm^2 $molec^{-1}$. Because of the way the scale factor is constructed (using the EPA data), comparisons using this baseline approach are meaningful only in terms of correlation statistics and not for comparing absolute concentrations.

Table S8: Comparison of model+OMI estimates of surface NO_2 with in situ measurements (fall data, n=1221)

Statistic	OMI[a]	OMI + CAMx	OMI + GEOS-Chem	CAMx only
Avg. difference (ppb)	N/A	-5.84	-10.59	-2.55
Avg. absolute difference (ppb)	N/A	7.17	10.81	6.02
Avg. bias (%)	N/A	-22%	-52%	17%
Avg. absolute bias (%)	N/A	49%	63%	56%
Pearson's correlation	0.76	0.76	0.70	0.77
Spearman's correlation	0.80	0.84	0.78	0.82
Kappa	0.40	0.46	0.39	0.44
Weighted-Kappa	0.60	0.65	0.58	0.63

[a]Assuming a constant scale factor of 1.0×10^{-15} ppb cm^2 $molec^{-1}$. Because of the way the scale factor is constructed (using the EPA data), comparisons using this baseline approach are meaningful only in terms of correlation statistics and not for comparing absolute concentrations.

Table S9: Comparison of model+OMI estimates of surface NO_2 with in situ measurements (winter data, n=637)

Statistic	OMI[a]	OMI + CAMx	OMI + GEOS-Chem	CAMx only
Avg. difference (ppb)	N/A	-5.80	-9.60	-4.12
Avg. absolute difference (ppb)	N/A	7.77	10.04	7.78
Avg. bias (%)	N/A	-16%	-37%	18%
Avg. absolute bias (%)	N/A	53%	56%	63%
Pearson's correlation	0.75	0.79	0.79	0.67
Spearman's correlation	0.79	0.82	0.82	0.77
Kappa	0.38	0.49	0.44	0.42
Weighted-Kappa	0.58	0.65	0.62	0.60

[a]Assuming a constant scale factor of 1.0×10^{-15} ppb cm^2 $molec^{-1}$. Because of the way the scale factor is constructed (using the EPA data), comparisons using this baseline approach are meaningful only in terms of correlation statistics and not for comparing absolute concentrations.

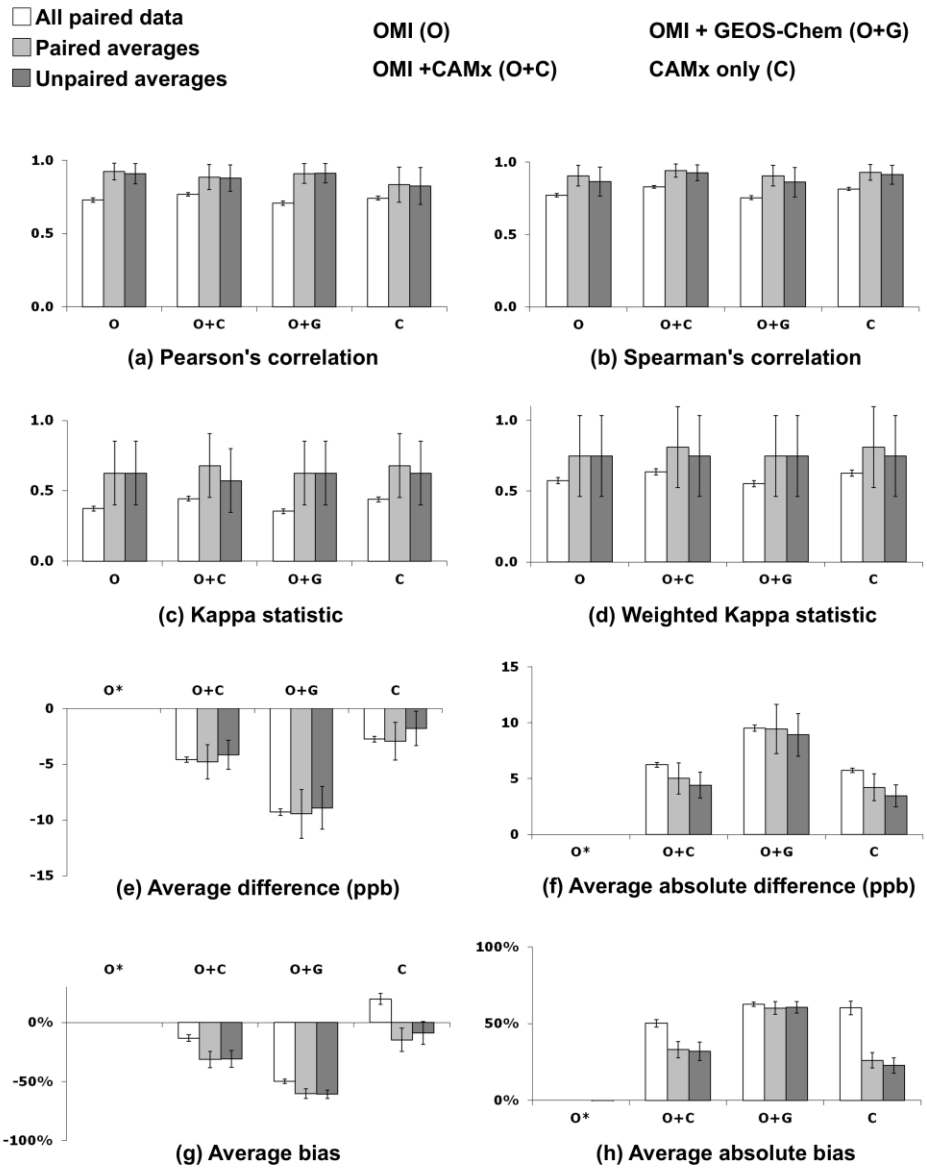

Figure S1: For surface NO_2 concentrations, comparison of in situ measurements and model+OMI estimates. "Unpaired average" is the annual average at each monitor for all available data (n=8666 for EPA monitors; n=4575 for OMI measurements). "Paired average" employs the annual average at each monitor for days with coinciding satellite and EPA monitor measurements (n=25). "All paired data" is the daily value at each monitor for days with coinciding OMI and EPA monitor measurements (n=4138). Error bars indicate the 95% confidence interval. Values shown in this figure are also in Tables S3-S5. Certain comparisons, marked with an asterisk (*) are blank: because of the way the scale factor is constructed (using the EPA data), comparisons using this baseline approach are meaningful for correlation statistics, not for comparing absolute concentrations.

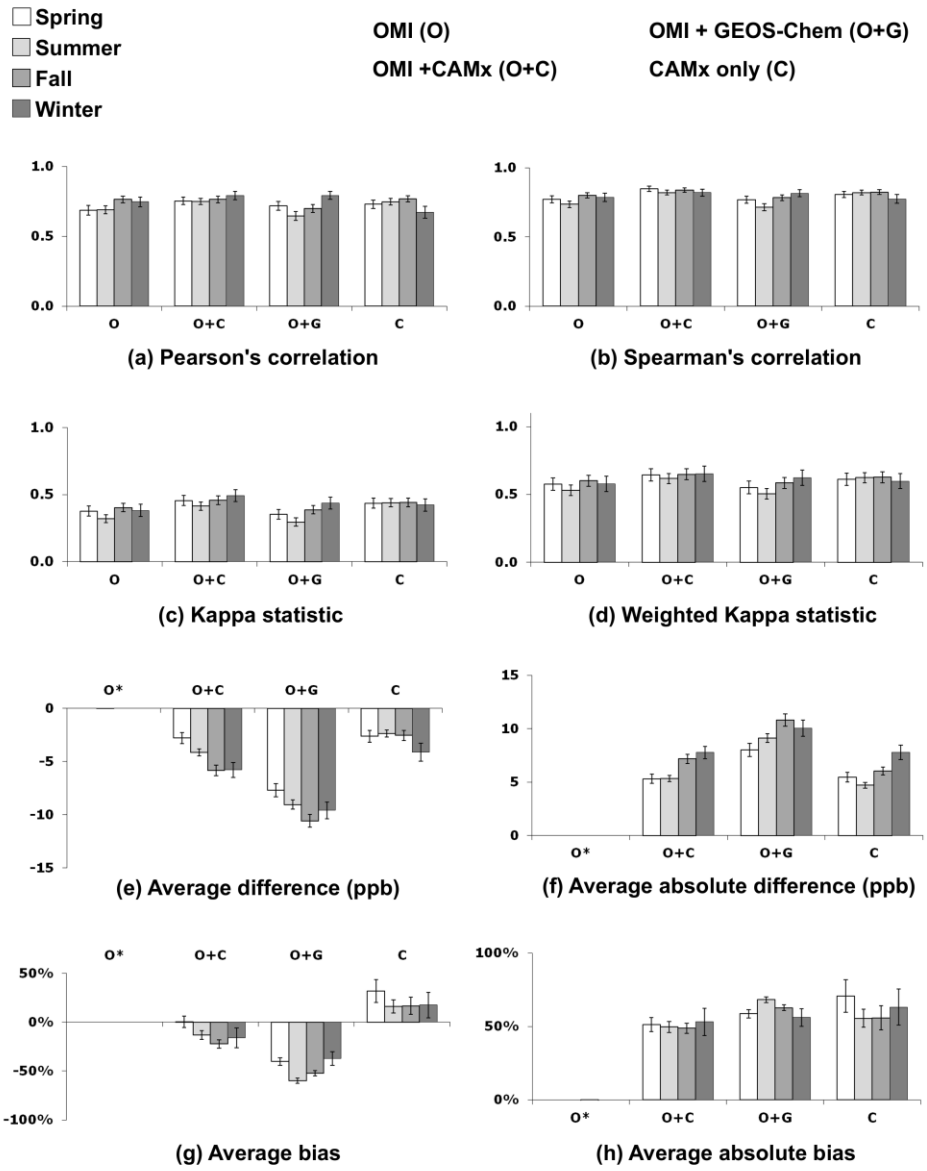

Figure S2: For surface NO_2 concentrations, comparison of in situ measurements and model+OMI estimates corresponding to spring (n=936), summer (n=1344), fall (n=1221), and winter (n=637). Error bars indicate the 95% confidence interval. Values shown in this figure are also in Tables S6-S9. Certain comparisons, marked with an asterisk (*) are blank: because of the way the scale factor is constructed (using the EPA data), comparisons using this baseline approach are meaningful for correlation statistics, not for comparing absolute concentrations.

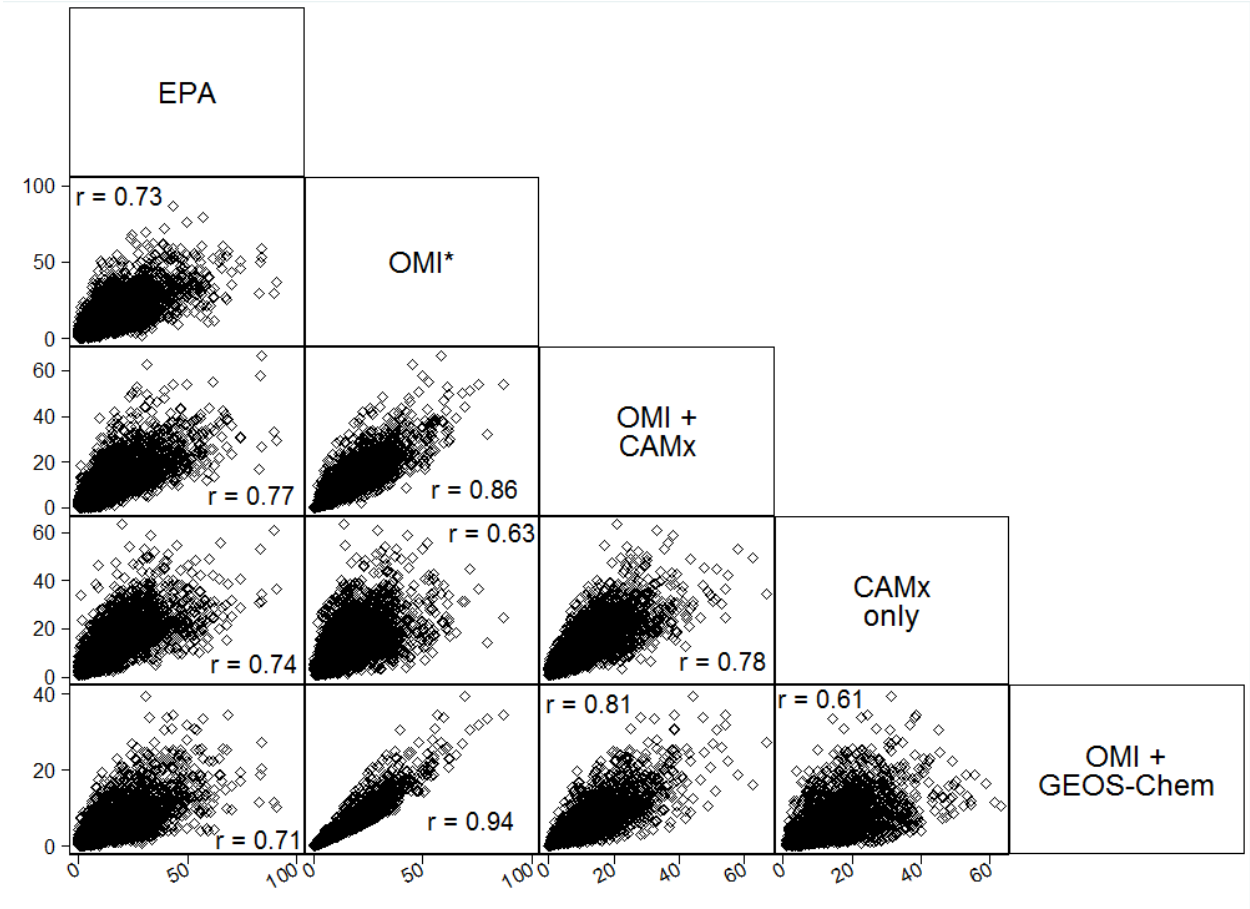

Fig. S3. Pair-wise scatter plots for paired daily NO_2 concentrations (ppb). Values in each box indicate Pearson correlation (r value). *Assuming a constant scale factor of 1.0×10^{-15} ppb cm^2 $molec^{-1}$.

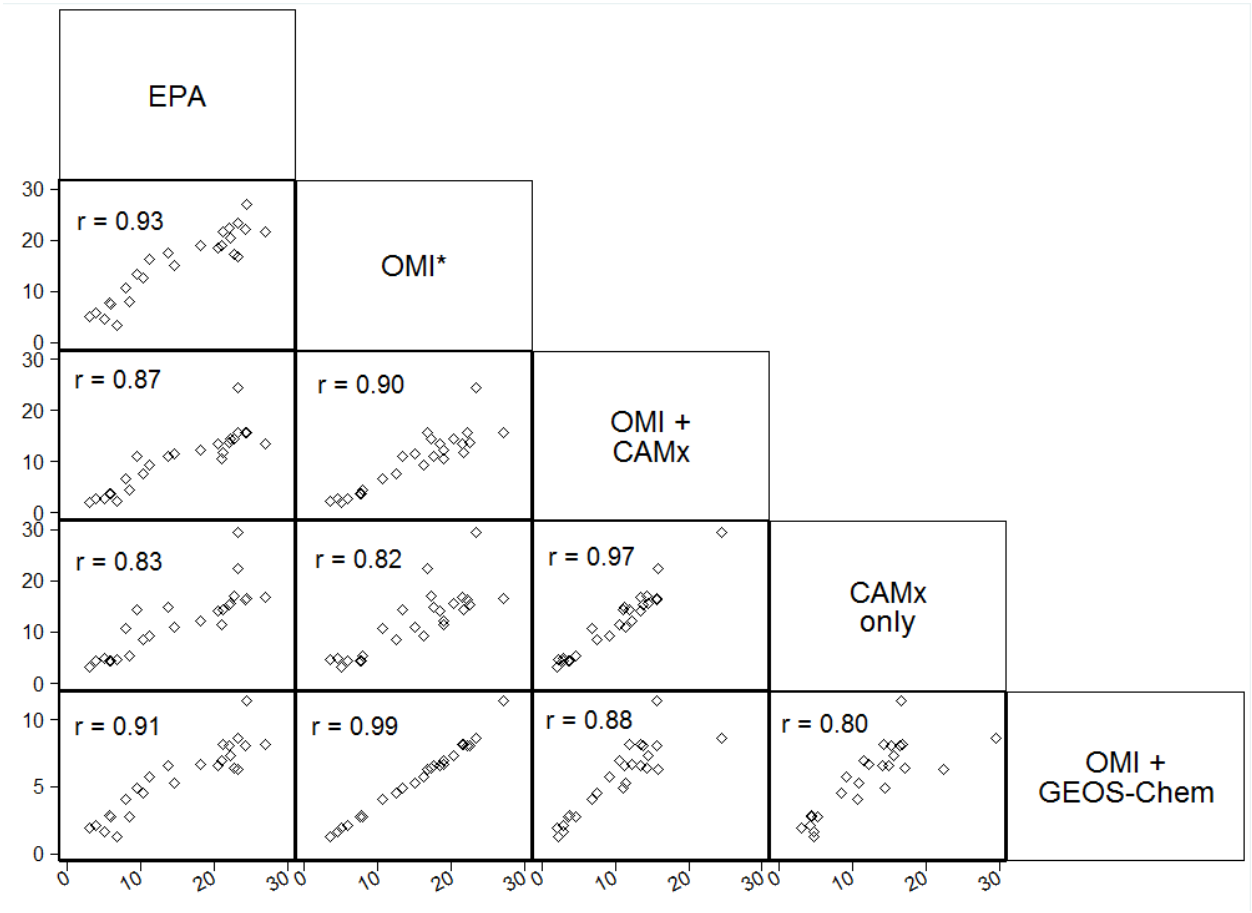

Fig. S4. Pair-wise scatter plots for paired annual average NO_2 concentrations (ppb). Values in each box indicate Pearson correlation (r value). *Assuming a constant scale factor of 1.0×10^{-15} ppb cm^2 $molec^{-1}$.

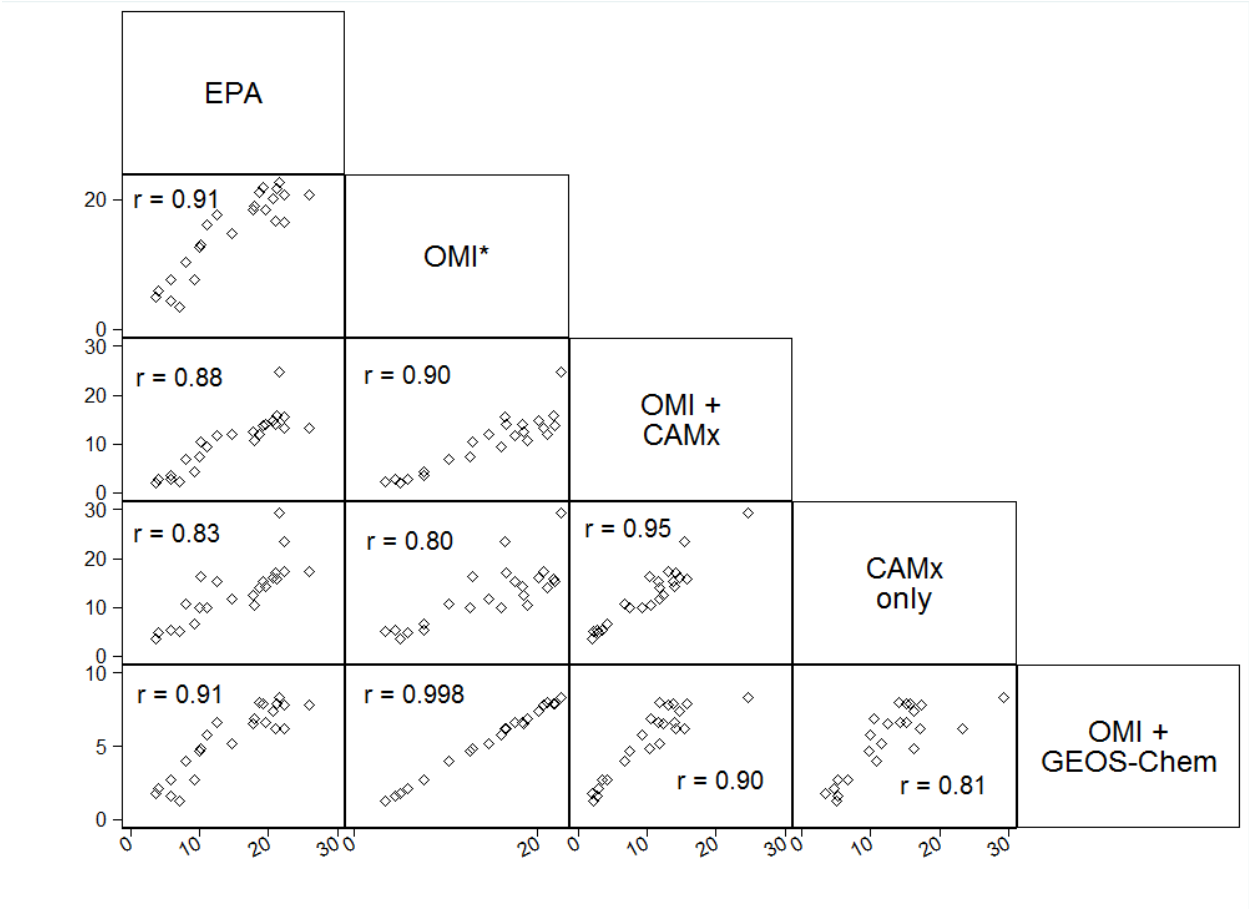

Fig. S5. Pair-wise scatter plots for unpaired annual average NO_2 concentrations (ppb). Values in each box indicate Pearson correlation (r value). *Assuming a constant scale factor of 1.0×10^{-15} ppb cm^2 $molec^{-1}$.